GSI-P-5-77
JULI 1977

DEEP INELASTIC COLLISIONS BETWEEN VERY HEAVY NUCLEI

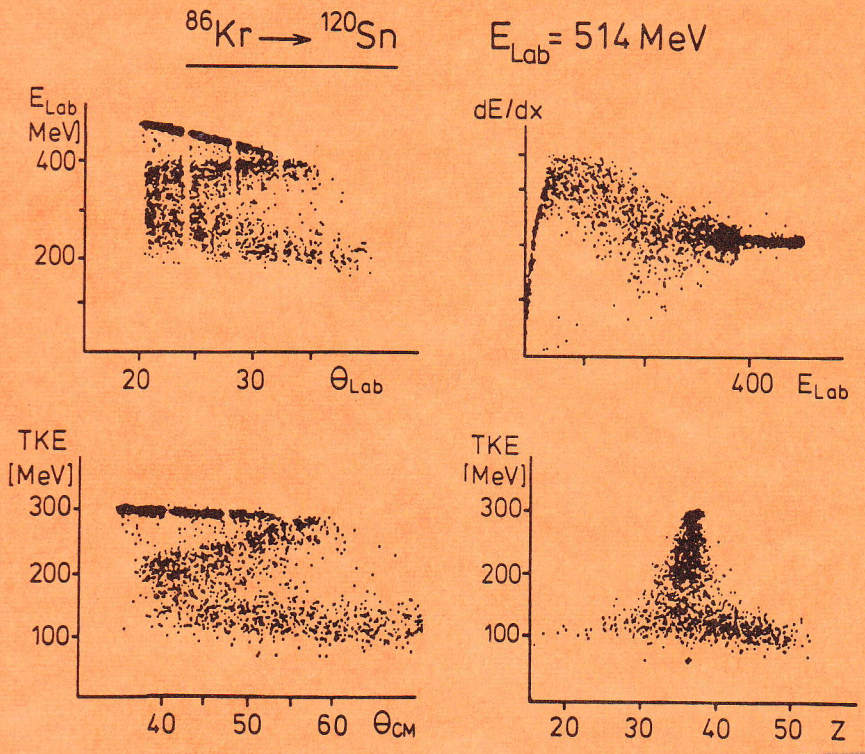

GSI-BERICHT P-5-77

GESELLSCHAFT FÜR SCHWERIONENFORSCHUNG MBH, DARMSTADT

GSI-P-5-77
JULI 1977

DEEP INELASTIC COLLISIONS BETWEEN VERY HEAVY NUCLEI

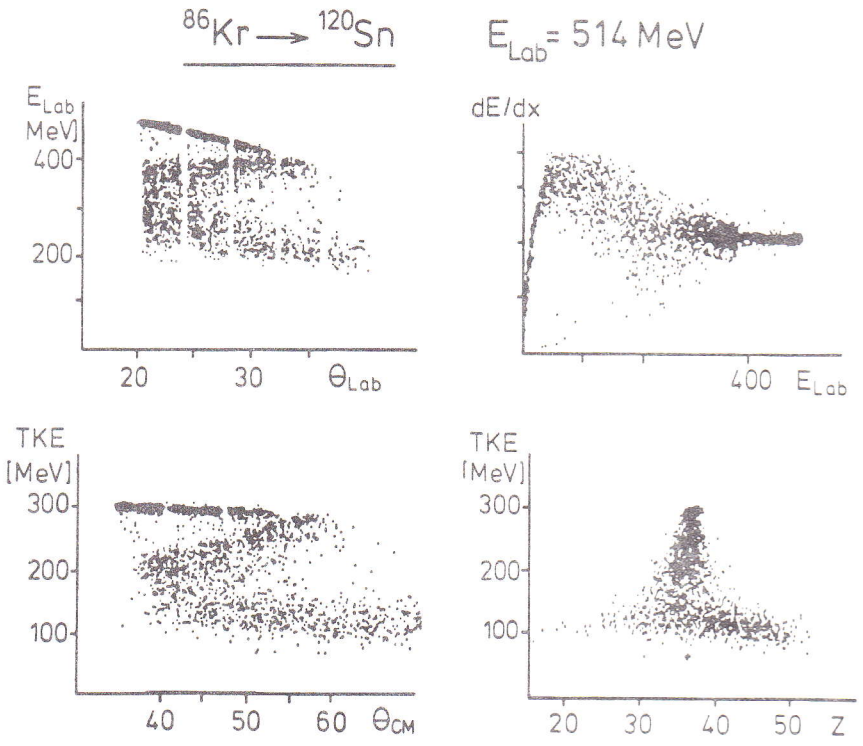

GSI-BERICHT P-5-77

GESELLSCHAFT FÜR SCHWERIONENFORSCHUNG MBH, DARMSTADT

DEEP INELASTIC COLLISIONS BETWEEN VERY HEAVY NUCLEI

H. Sann, A. Olmi, Y. Civelekoglu, MPI für Kernphysik Heidelberg

D. Pelte, Universität Heidelberg

U. Lynen, H. Stelzer, A. Gobbi, Y. Eyal[+], W. Kohl, R. Renfordt, I. Rode, G. Rudolf[*], D. Schwalm, R. Bock, GSI Darmstadt

Introduction

One and a half years ago the UNILAC accelerator started to deliver heavy ion beams of 5.9 MeV/amu, which is a sufficient energy to overcome the Coulomb barrier and so to study nuclear interactions. Today, bombarding energies up to 8.5 MeV/amu are commonly available for a variety of beams including the very heavy projectiles like uranium and lead. This unique facility has opened up at GSI during the past year a broad spectrum of activities including the search for superheavy nuclei, for the spontaneous emission of positrons in the overcritical electric field, for yrast traps, etc.

What we shall report here will be on the shadow side of these real highlights, but if one thinks of the moon, the back side is as interesting as the enlighted one. The present talk will concentrate on a survey study of deep inelastic collisions and will not at all reflect the general spectrum of activities at GSI (GSI 76). The reactions investigated are summarized with a number of characteristic quantities in table. 1. It is a survey study performed for a wide span of targets and projectiles so as to recognize the general features of the collision and their trends, while moving from the already known lighter systems to the heaviest possible target projectile combination U on U.

Several symmetric ingoing channels (Xe-Sn, Pb-Pb and U-U) were chosen as well as a number of asymmetric systems (Kr-Sn, Kr-Er, Xe-Au, Xe-U, U-Pb). The original 5.9 MeV/amu were not sufficient to reach the Coulomb barrier for the heaviest combinations and it was only at the end of 1976 that we were able to move on into the new region. Taking advantage of what we learned from this general survey we have recently started to investigate some more specific questions by observing the γ-multiplicity and the bombarding energy dependence of the deep inelastic process (Kr-Sn, Kr-Er).

Table 1 shows that the Coulomb barrier is typically exceeded by a factor of 1.3; in the energy dependent study we scan a region between

[+]) On leave from Weizman Institute, Rehovot, Israel

[*]) Humboldt fellow, on leave from CRN Strasbourg, France

Table 1: List of the reactions investigated

Proj	Target	E_{Lab} (MeV/amu)	E_{CM} (MeV)	E^* (MeV)	E_{CM}/E_{Coul}	l_{max} (h)	η' +)
^{86}Kr	^{120}Sn	4.9	250	50	1.24	140	375
		5.99	300	99	1.50	199	265
		7.2	360	160	1.80	252	208
		8.2	411	210	2.04	289	182
^{86}Kr	^{166}Er	4.9	283	25	1.10	112	711
		5.99	339	81	1.32	203	397
		7.2	407	150	1.58	276	293
		8.2	464	206	1.80	323	249
^{132}Xe	^{120}Sn	5.9	370	90	1.32	227	516
	^{197}Au	7.55	596	184	1.47	402	571
	^{208}Pb	7.55	610	190	1.46	412	583
	^{238}U	7.55	641	118	1.40	423	831
^{208}Pb	^{208}Pb	7.5	780	188	1.32	499	702
	^{238}U	7.5	832	183	1.29	521	798
^{238}U	^{238}U	7.5	892	180	1.26	546	956

1.1 and 2. The corresponding kinetic energy above the Coulomb barrier, after the nuclei have already been slowed down in the Coulomb field is typically between 100 and 200 MeV: this is roughly the total kinetic energy available for the internal excitation of the interacting nuclei. The maximum angular momentum in the relative motion for grazing partial waves, is of the order of 200 to 500, and even if only a certain fraction (~2/7) can be absorbed, a large amount of angular momentum is also available to the internal degrees of freedom of the nuclei.

The variety of kinetic energies and target projectile combinations available make of these reactions a powerful tool to study many average properties of nuclear matter, while the interacting nuclei are strongly overlapping. From this point of view we are pursuing to the heavier systems the interesting investigations of the deep inelastic reaction and of the diffusion mechanism previously studied at Orsay (Le76, Ga76, Ng77), Berkeley (Hu77, Mo76) and Dubna (Ar 73). Typical to these reactions is, among other aspects, the increasing classical behaviour reflected by the Sommerfeld parameter η' and the vanishing fusion cross section, so that the whole total cross section undergoes the deep inelastic process. Also characteristic of the heavier systems is the presence of fission as a possible

+) η' is evaluated using the relative velocity at the Coulomb barrier.

decay mode of the excited primary products after the collision: this is usually called the sequential fission.

Summarizing, the general interest of this study lies in the reaction mechanism and the mass diffusion process, without forgetting possible nuclear structure effects. Expecially interesting is to investigate the mass transfer process for the heaviest systems (U on U), into the transuranic region, to determine the primary population probability as well as the decay properties of these nuclei.

The content of the report will be subdivided as following:

1. Experimental device.
2. A systematic study of the deflection function: a direct test of nuclear forces.
3. The nuclear diffusion process between heavy nuclei.
4. Results of the γ-multiplicity measurements.

1. The experimental device

The kinematic coincidence apparatus is schematically illustrated on fig. 1. A position sensitive ionisation chamber (Sa 75) is centered at the grazing angle of the reaction and is used as a trigger counter. For each particle the chamber measures scattering angle (x, y-read-out), total energy, energy loss and time of arrival. The distance from the target is 1 m, the substended solid angle 50 msr.

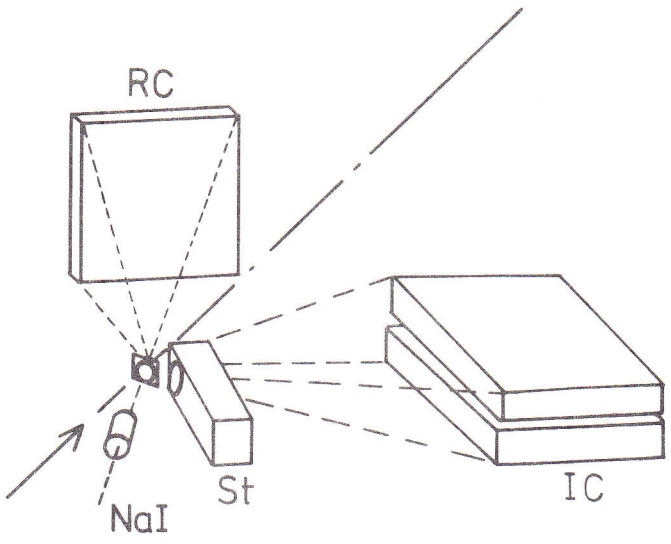

Fig. 1: Experimental apparatus. IC ionisation chamber RC recoil counter, St start detector, NaI 3"x3" sodium idide crystal.

The start signal is delivered by the secondary electrons ejected from a thin carbon foil placed 7 cm from the target: the electrons are amplified in a channel plate after deflection in a magnetic field (Re 77).

On the opposite side of the ionisation chamber a 250 msr detector (St 77) observes the particles emitted in the direction of the recoiling nuclei: it consists of a multiwire proportional counter which measures scattering angles (x-y-coordinates) and energy loss. It is followed by parallel plate detectors which deliver a stop signal.

Up to 3 NaI crystals were used to determine the γ-multiplicity in coincidence with the trigger counter information.

The data obtained up to now were collected during a total running time of 7 days. Most of the information, extracted from the data was gained from the ionisation chamber. The determination of scattering angle and

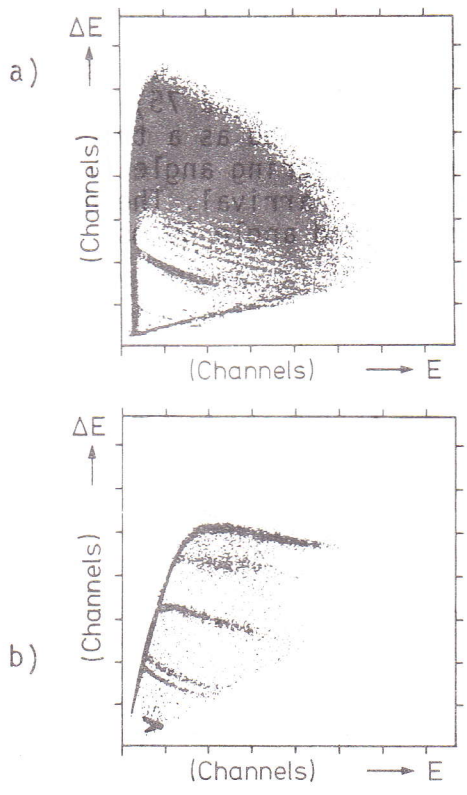

Fig. 2:

Two dimensional plots of energy loss versus total energy. In part a) are displayed light elements below Z ≃4o, while in part b) from the top to the bottom the elements Pb, Ho, Sn Cu, Fe and Al can be recognized.

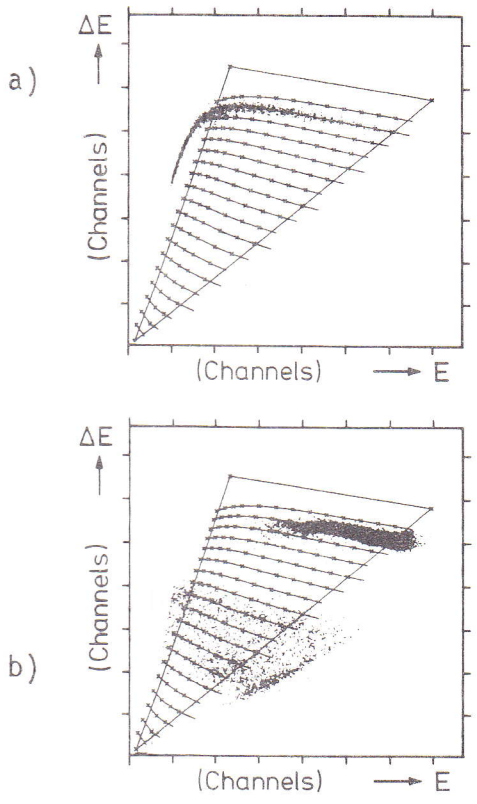

Fig. 3:

Proton number identification.
Only the events inside the triangle are identified. On the outside, to the right, are seen the particles which are not fully stopped in the ionisation chamber.

total energy is quite straightforward, while the Z identification is more elaborated; it follows in the usual way from the relation between energy loss and total energy deposited in the counter. Fig. 2 shows two energy loss vs energy plots. The single charges can be resolved up to about Z=35 (fig. 2a), which is a good resolution considering the large aperture of 40 x 6 cm^2 of the counter. For the heavier systems, where the single charges are no more distinguishable, we found very useful to take, as calibration lines, the recoiling products emerging from thick wires of different elements hit by the beam (fig. 2b). In figure 3a is shown how we first matched a grid to the measured calibration line. The grid is calculated on the basis of a semiempirical dE/dx formula and then used to interpolate the data and extract the Z values for each event (fig. 3b). At present the shape of the dE/dx curve for a given Z is well reproduced by the formula, however, the spacing between adjacent Z for Z > 75 is found to deviate from the extrapolation based on the light elements: additional calibration work is in progress. The data of figure 3b are obtained from the U-U collision. Such a Z identification is essential in order to determine small deviations from the proton number of the projectile, while investigating the nucleons diffusion process.

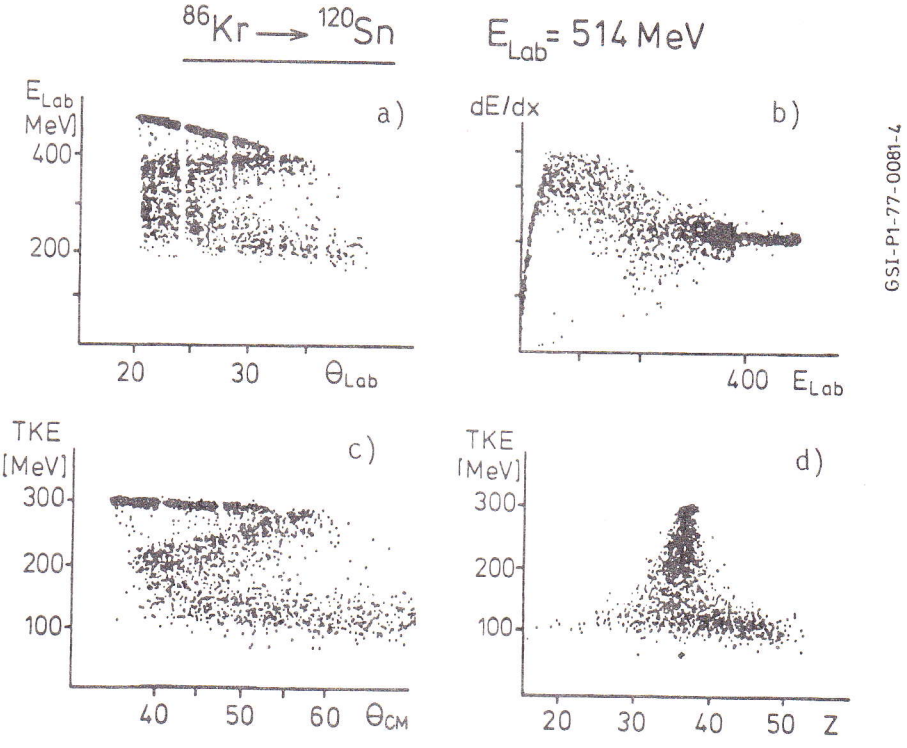

Fig. 4: On-line results from the storage display.

The plots of fig. 4 will demonstrate the advantages of the experimental device when applied to the deep inelastic reactions. The results of the Kr on Sn reactions are shown as they appear, on the storage display, during the data acquisition after 5 minutes of accumulation. The same event is plotted twice: in an energy loss vs total energy (fig. 4a) and in a total energy vs laboratory angle plot (fig. 4b). Through the density of the accumulated points it is easy to recognize the correlations between the 3 measured quantities. At small scattering angles emerges a strong elastic scattering: the energy decreases toward larger angles because of the kinematic dependence in the laboratory system for the elastic process. The empty spaces originate from the window support of the gas counter. At the grazing angle, where the nuclear interaction starts, the elastic scattering drops drastically in intensity. Just before the grazing angle, the increasing attractive nuclear forces constrain the scattered particles on a trajectory toward smaller angles (fig. 5). At the same time, due to the nuclear interaction, the nuclei are excited. This takes energy from the relative motion, the observed kinetic energy drops continuously as the excitation energy increases. This is how the deep inelastic process develops, coming from the elastic, partly damped going to the deep inelastic component. The events, which have a laboratory energy smaller than 300 MeV can be attributed to the fully relaxed component. It is not possible to tell directly from these data what is the deflection angle of the fully relaxed or so called orbiting component: if it has been scattered from the same side of the nucleus as the partly damped component, if it comes from a negative angle trajectory, or if the composite system has already made many turns as in the fusion fission process. As we shall see later, such a question cannot be answered in general for all systems and, even for a given system different contributions may be present at once.

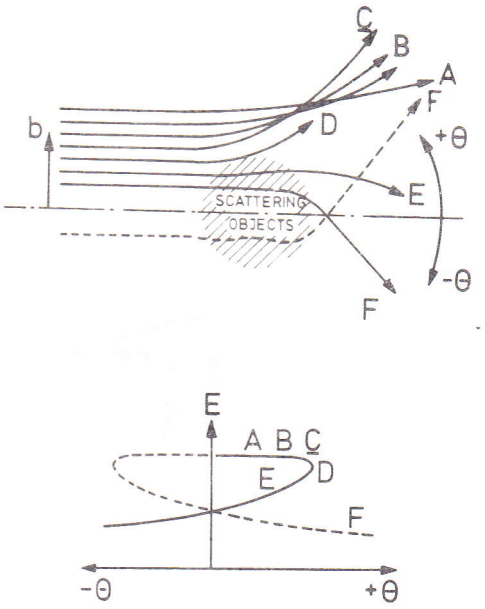

Fig. 5: The different trajectories of a Wilczynski diagram (Wi 73).

A complementary information on the mass diffusion is obtained from the ΔE vs E diagram of figure 4b. For decreasing energy we observe a spreading and a shift on the ΔE scale, which correspond to an increased mass diffusion as the nuclei are excited, with a tendency to populate a symmetric fragmentation of two roughly equal nuclei.

This is not only a quite efficient way to accumulate data, but it also makes possible to follow continuously the evolution of the distributions and, in a few minutes, to recognize the main features of the collision process for a given target projectile combination at a given bombarding energy. This type of representation underlines the continuity of the whole process from the grazing collisions to the compound nucleus formation: this is certainly a challenge for a general scattering theory.

The three measured quantities Θ, E, Z are sufficient to transform the two body kinematic quantities from the laboratory into the CM system. The mass is deduced from Z over a 1 to 1 correspondence, which follows the β-stability valley. The light particles evaporation is neglected in the transformation.

The results of the event by event transformation are shown on part d) and c) of figure 4. The new calculated quantities are the total kinetic energy TKE and the center of mass scattering angle Θ_{CM}. The so called Wilczynski diagram (Wi 73) is obtained by plotting TKE vs Θ_{CM}. From such a representation it is easy to read out the energy of the relaxed component, which corresponds roughly to the repulsion energy of the Coulomb barrier. The TKE vs Z diagram illustrate again the charge diffusion with a tendency toward symmetry. While considering the data in the CM system, it should be remembered that the limited range of observation in the laboratory introduces diffuse cuts on the distributions. The recoiling nuclei are usually not detected because their grazing angle in the laboratory system is out of the observation range of the detector and even if they hit the detector their kinetic energy is so low, that it is very hard to identify them.

In the following we shall study the evolution of the deflection function from the elastic to the fully relaxed component for six different systems. This will clarify the relative motion of the colliding heavy particles. Afterwards we shall consider, for the same systems, the evolution of the proton number as a function of the total kinetic energy loss (TKEL) and this will illustrate the mass diffusion process overimposed on the motion of the colliding objects.

2. A systematic study of the deflection function

Figure 6 shows three asymmetric Kr-Er, Xe-Au, U-Pb and three symmetric systems Xe-Sn, Pb-Pb and U-U. They are ordered for increasing strength of the Coulomb repulsion. The Coulomb barrier is exceeded by a factor of 1.25 to 1.4 which is a lower value as the 1.5 of the Kr on Sn system of figure 4. This explains the absence of an orbiting component (MO 76).

With Kr on Er and Xe on Sn we compare an asymmetric (fig. 6b) with a symmetric ingoing channel (fig. 6a) at the same total energy of the composite nucleus. They both display a quite similar trend: the nuclear attraction takes the upper hand against Coulomb repulsion; the particles are constrained to smaller scattering angles, while the overlap increases.

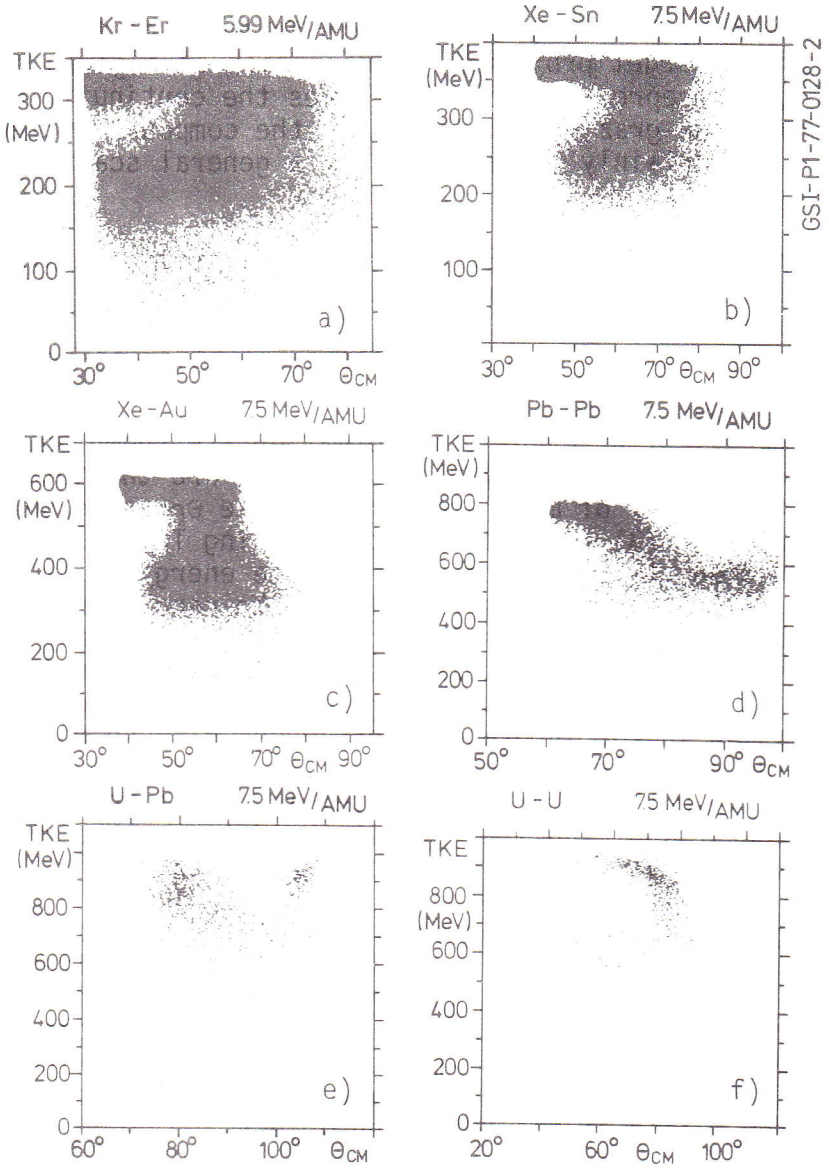

Fig. 6: Wilczynski diagrams of 6 different reactions.

Moving on toward stronger Coulomb fields the Xe on Au scattering (fig. 6c) shows a particular balance between repulsive and attractive forces: the particles are scattered around a fix mean angle value. This is usually called the focusing effect (Hu 76). In the next heavier system Pb on Pb (fig. 6b) we observe a monotonic increase of the scattering angle for increasing TKEL. Because of the identity of the ingoing particles, we observe two distributions symmetric about 90^0 (CM), which cross at 90^0. The same behaviour is also present in the U-Pb system (fig. 6d). From the left to the right we observe how the Pb component develops; in the right upper corner we see the uranium

component which should, in principle, be mirror symmetric about 90° to the lead component. Because of the sequential fission, the highly excited uranium-like nuclei, which have low kinetic energies, are missing in the diagram. Therefore, in the asymmetrich U-Pb system, it is possible to distinguish the projectile-like from the recoil-like-nuclei and the trends are more readily recognized.

In the U-U-scattering we observed, as it will be shown in same details later, a dominance of the sequential fission: this can already be anticipated form the Pb-U interaction. The Wilczynski plot is shown in fig. 5e for selected ternary processes, by requiring a coincident fission fragment in the recoil counter. In this way it is possible to drastically reduce the elastic events, which otherwise would overwhelm the plot. It seems that the general trend of the deflection function towards larger scattering angles is still present in the U-U-scattering, although very few events survive the sequential fission at high excitation energies.

From the observation of figure 6 we deduce that a gradual trend exist, where between the lighter systems (Kr-Sn) and the heavy systems (Pb-Pb) the deflection function, after the first rainbow but before the grazing angle, possibly describes a second rainbow angle (De 75): this second rainbow angle moves toward larger angles for the heavier masses. In addition the relation between impact parameter and scattering angle seems to be washed out in the fully relaxed component.

The general interest of these deflection function studies can be summarized in two main points:

1. Test of nuclear forces: Through the delicate balance between Coulomb, centrifugal and nuclear forces of the rotating dinuclear molecular system (fig. 7) it should be possible to deduce form the known Coulomb and centrifugal forces the nuclear attraction as a function of the strength of the overlap integral. The important degrees of freedom to be considered are besides the dependence from the impact parameter, the time dependent changes of the overlap integral because of deformations, and the change of the centrifugal forces because of tangential frictional forces during the slowing down process. This dynamical situation of the dinuclear molecular system is also essential to understand the limits onto the compound nucleus formation.

   One interesting aspect of this inverse scattering problem for the reconstruction of the interacting potential, is the fact that there is no missing cross section over a large range of observation; so there is no absorption, we are observing all elements of the scattering matrix. In this sense we have a situation very different from an elastic scattering study of the interaction potential where only one single channel is investigated and where the absorption

prevents the analysis of the interior. The price to be paid comes from the superposition of the mass diffusion process on top of the relative motion process, so that both are intimately correlated and cannot be easily unfolded. The mass diffusion will be treated in same details in the next chapter.

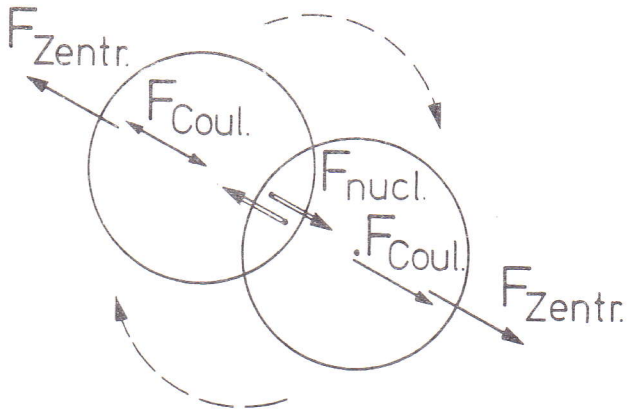

Fig. 7: The rotating dinclear molecular system

2. Determination of the time scale of the interaction: The interaction time can be obtained from the scattering angle thorugh an integration along the trajectory of the relation

$$l_{rel} = I \cdot \frac{\Delta\Theta}{\Delta t}$$

which describes the angular velocity of the dinuclear molecule (Hu 77, Nö 76). The moment of inertia I(t) depends on the shapes the system assumes. The relative angular momentum $l_{rel}(t)$ depends on the internal spin absorbed by the fragments. The trajectories of the U-U collision are illustrated in figure 8. Part a) considers a grazing situation, while part b) shows a fully damped collision at small impact parameters. The scattering angle is roughly the same in both cases but the nuclei are mostly deflected in the Coulomb field for a peripheral collision and in the overlapping nuclear field for the central collision. We expect from this consideration the U-U interaction time to be similar to the one of the Xe-Bi reaction analyzed in some details by Huizenga (Hu 77), which is of the order of 10^{-22} to 10^{-21} sec. The knowledge of such a time scale is important for the prediction, through the diffusion model, of the strength of the mass transfer in the transuranic region.

The derivation of a time scale can be of considerable help not only in understanding the diffusion process but also the relaxation phenomena of the various degrees of freedom.

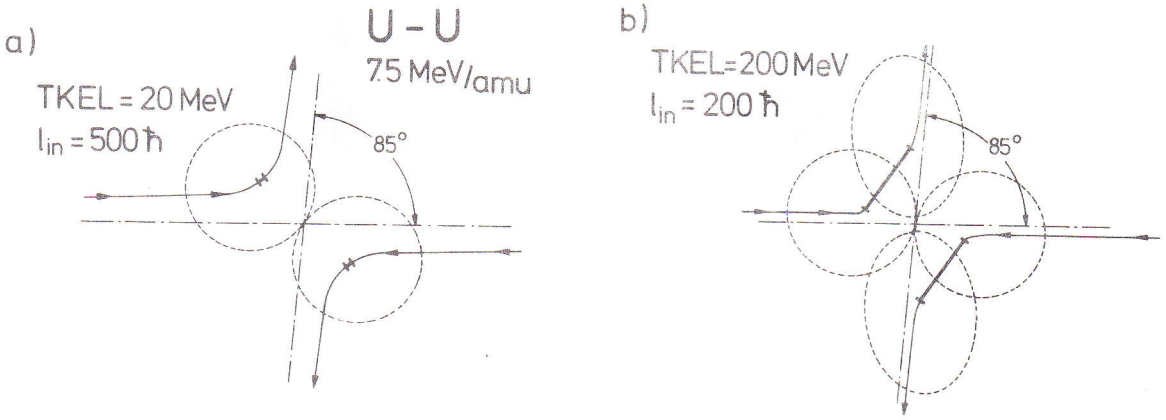

Fig. 8: The trajectories in the U-U collisions.

3. The diffusion of nucleons between heavy nuclei.

Figure 9 illustrates the evolution of the nucleons diffusion as a function of the loss on total kinetic energy. The same symmetric and asymmetric systems of figure 6 are reconsidered. The Xe on Sn reaction shows a nice symmetric distribution, which monotonically widens as the kinetic energy decreases. The corresponding asymmetric ingoing channel shows a preferential population of the heavier masses: this is usually called a driving force toward symmetry. The Xe on Au combination behaves very similarly to Kr on Er. A weak component of the sequential fission of Au is seen at low kinetic energies. If the Pb-Pb distributions are compared to the Xe on Sn case, one observes a shift to the lower proton numbers. The same trend is present on the U-U case, although few events are observed at the high excitation energies. The same is also true in the U-Pb scattering,which directly illustrates the drastic change taking place for the heavy masses above lead. From potential energy surface we would expect that the primary masses produced in the Pb-Pb, and U-U interaction would be similar to the Xe-Sn interaction. The question to be discussed later will be if the sequential fission can explain the missing part of the Z distribution for the heavier elements. Before investigating these questions let us understand better the lighter systems where the decay of the primary excited masses is limited to the neutron evaporation, so it doesn't alter the Z distribution.

Until now we have been rather qualitative in the description of the data, the following figures shall give a quantitative representation of the results after normalization to the Rutherford cross section. Instead of the usual $d\sigma/d\Omega$ we have chosen a $d\sigma/d\theta$ representation, because the later is proportional to the total reaction cross section when the whole angular range is observed. Figure 10 displays the

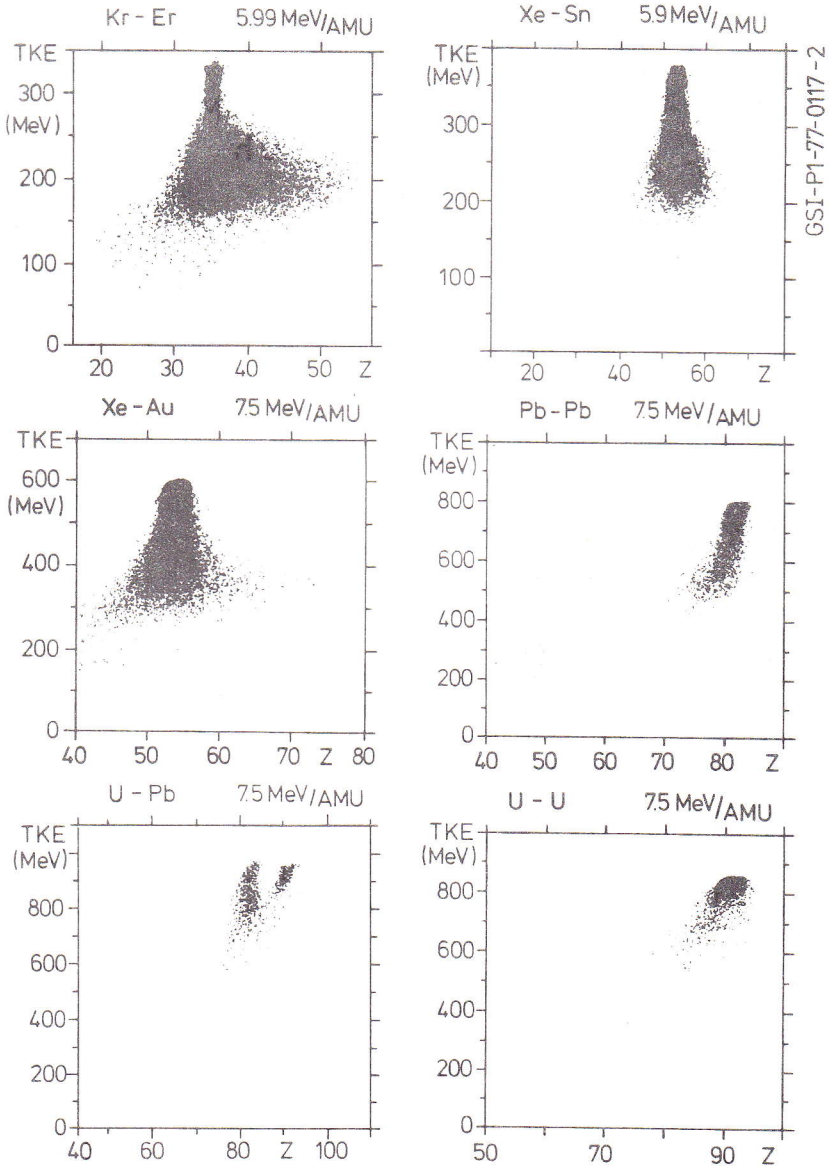

Fig. 9: The nucleons diffusion as a function of the TKEL. The distributions are measured for a given setting of the position sensitive ionisation chamber, which is centered around the grazing angle of the reaction and observes the projectile-like fragments. The recoil-like fragments are observed partially in the U-Pb reaction.

absolute cross sections for the Kr on Er reaction. The proton number- and angular-distributions are shown on a logarithmic scale for several cuts as a function of the total kinetic energy loss (TKEL). For lower excitation energies the Z-distribution is narrow as well as the angular distribution. As we move up in energy, we observe a broadening and an increasing slope on the heavy element side above the

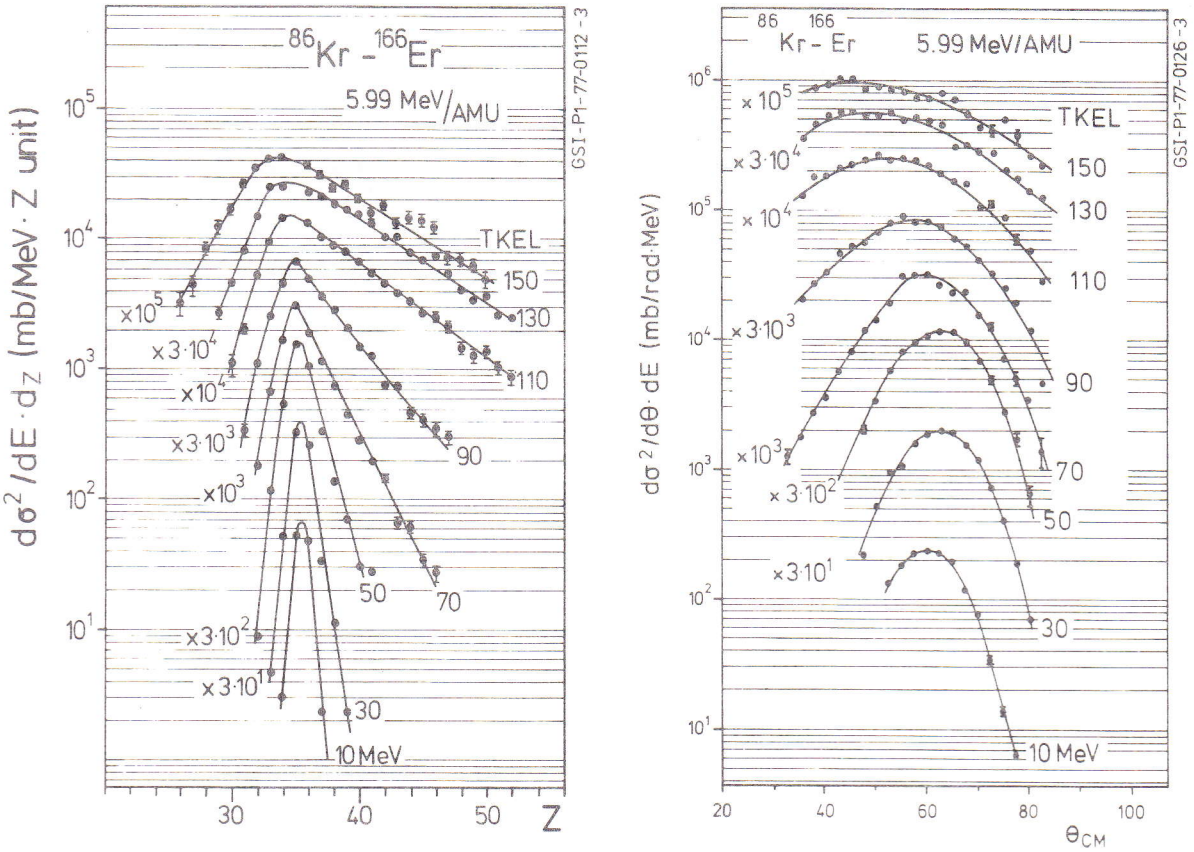

Fig.1o: Absolute differential cross sections of the Kr-Er collision. The number to the right of each Z-distribution indicates the average total kinetic energy loss of the considered events. The number displayed to the left is the scaling factor. If all reaction products would be observed and identified, symmetric Z-distributions (about Z=52) would also be observed, centered at the Z of the recoil products (Z=68).

Z-value of the projectile; we observe a shift and a broadening for the angular distribution. These are the same general features considered before on the two dimensional plots of the Wilczynski- and of the diffusion-diagrams (fig. 6 resp. 9).

What we want to learn now on a quantitative scale is how the width of the distributions, the σ_Z^2 value, changes as a function of the TKEL, as suggested by Huizenga in his systematic work (Hu 76) for a number of similar systems. We want to investigate if there is a general relation followed by the mass diffusion process.

It is rather instructive to compare the symmetric Xe-Sn system to the asymmetric Kr-Er system (figure 11). The Xe on Sn distributions remain Gaussian in shape, fully symmetric independently from the TKEL: the system is symmetric from the beginning and there is no driving force

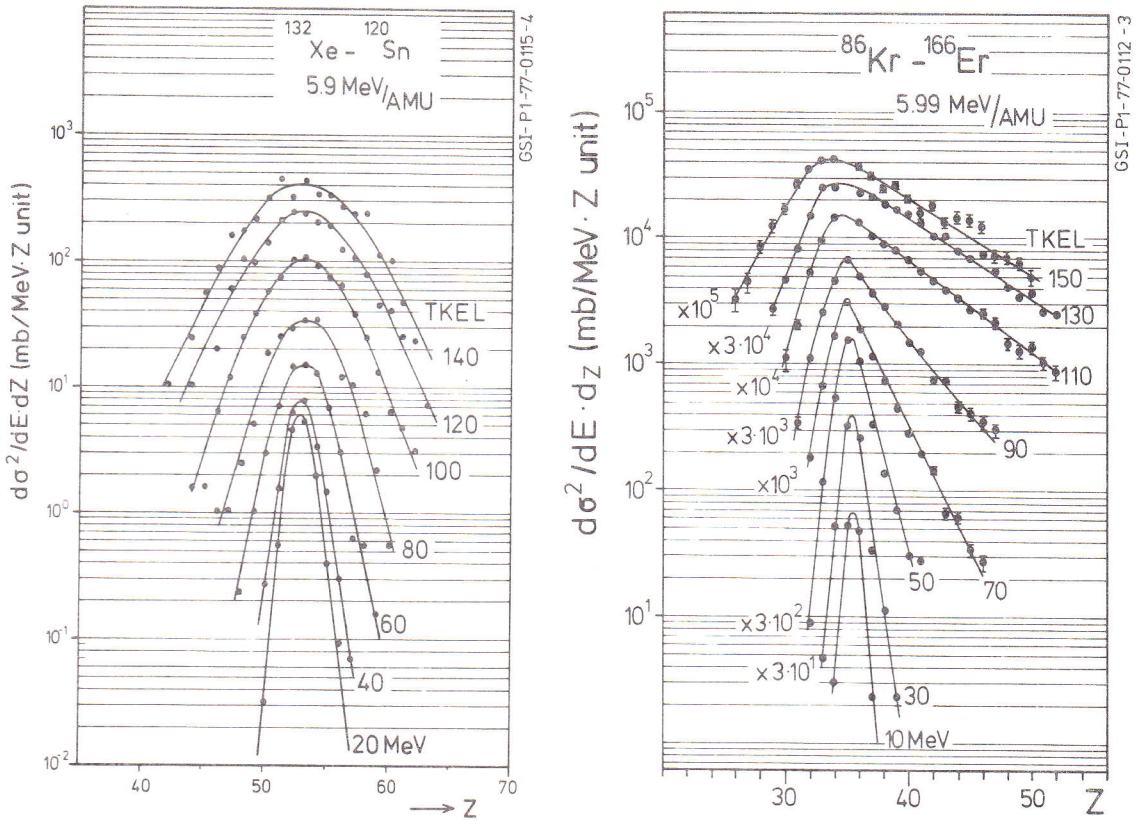

Fig.11: Comparison of the protons diffusion in a symmetric and asymmetric system. For the Xe-Sn reaction the scaling factor is always a multiple of $\sqrt{10}$.

expected from a potential energy surface; the centrifugal barrier tends to conserve the symmetry. There are good reasons to study symmetric, as well as asymmetric ingoing systems. The symmetric case dispalys a number of simplifying features. Let us compare these experimental results to the most simple form of a diffusion theory. We assume a frozen geometry between two overlapping nuclei and we apply the transport theory with the Fokker Planck equation as suggested by Nörenberg (Nö 76). It gives the proton number occupation probability as a function of time

$$P(Z,t) = (4\pi \cdot D_z \cdot t)^{-1/2} \exp\left[-(Z-Z_0-v_z \cdot t)^2 / 4 \cdot D_z \cdot t\right]$$

where v_z is the charge drift coefficient and D_z the diffusion coefficient. The measured variance σ_z^2 of the proton number distribution is related to the drift coefficient by

$$\sigma_z^2 = 2 \cdot D_z \cdot t$$

In this picture, for the Xe on Sn reaction, v_z is approximately zero and we test the diffusion coefficient D_z alone. In the framework of this model it seems difficult to explain why, in the Kr on Er

reaction we observe only a change in the skewness of the Z distribution without a drift of the centroid value: we observe that the cuts on TKEL do not sample only a given time intervall, overlap strength and impact parameter, but that these Z distributions may possibly come from a superposition of the different components of figure 12, with changing weighting factors. The unfolding of a time scale and the association of given impact parameters to well defined TKEL appear to be quite difficult in these cases.

The Xe on Au results of figure 13 represent also, for different reasons, an interesting piece of information. Like in the Kr-Er system, we observe a broadening and a decreasing slope as the TKEL increases, but in addition notice the puzzling shift of the maximum in a direction opposite to the one expected from a driving force toward symmetry which is predicted from simple liquid drop model consideration. We believe that this is due to a shell structure effect where both Xe and Au feel a coherent driving force toward close shells: Xe toward Z=50 and Au toward Z=82. These observations are

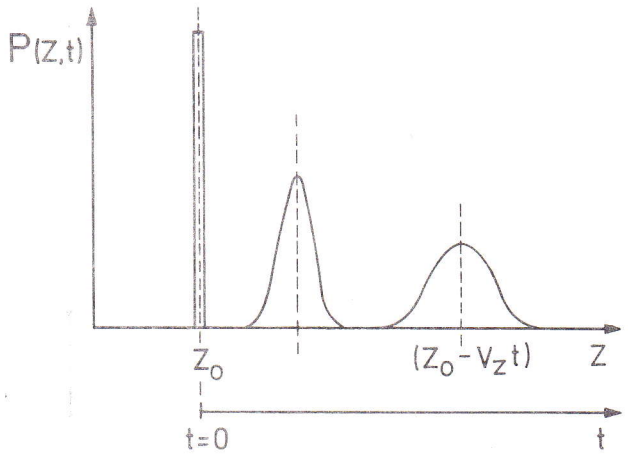

Fig.12: Predictions of a simple diffusion model.

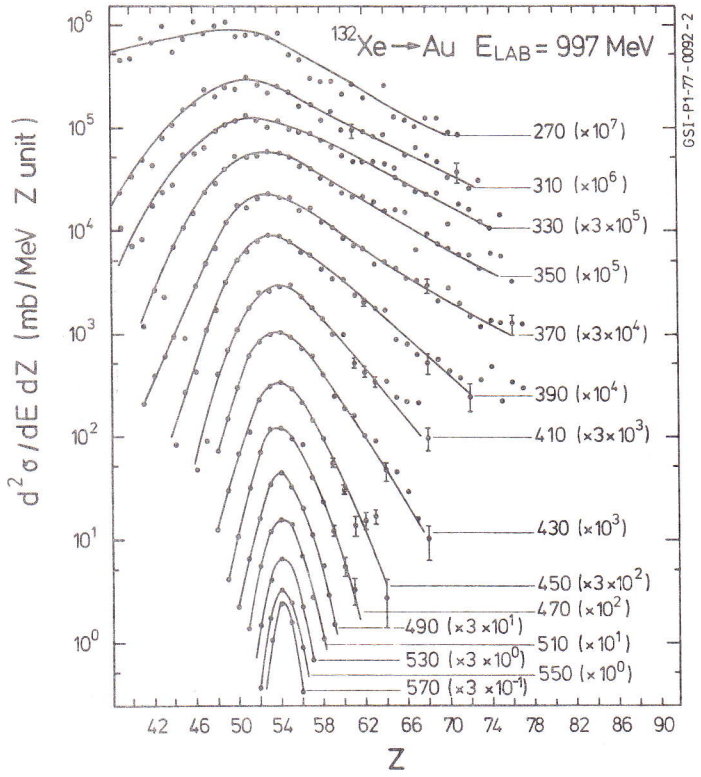

Fig.13: Center of mass data ($d\sigma/d\theta$) of the Xe-Au interaction. The TKEL value is indicated on the right of each distribution: the number in parenthesis is the scaling factor. For large energy dumping the calculated TKEL could be affected by the γ-evaporation of the excited fragments.

consistent with recent radiochemical measurements of Kratz et al. (Kr 77) where both light and heavy fragment were observed. It can nevertheless not be completely ruled out, at this point, that a light charged particles evaporation also contributes to the observed shift. However, these results are certainly of considerable interest and should stimulate additional experimental and theoretical work because the Xe on Au systems display optimum conditions for the observation of shell structure effects.

The next question to be considered is how the Xe-Sn, Kr-Er and Xe-Au results do fit into the present general understanding of the mass diffusion as investigated by Huizenga (Hu 77). The next figure (14) gives the relation between the variance σ_z^2 of the proton number distribution and the TKEL.

The results of the original Berkeley measurements are summarized by the full line. It should be pointed out that for the Berkeley data the Coulomb barrier is exceeded by 200 to 270 MeV, while for Kr on Er the total available kinetic energy was 85 MeV, for Xe on Sn 95 MeV and for Xe on Au 190 MeV. The comparison shows that all measurements roughly match on the TKEL scale as long as the energy dumping has not reached the fully relaxed component. It is also interesting to compare these same results in terms of a simple friction model (one body dissipation model) along the same line followed by Huizenga, where the rate of energy dissipation per unit of time is proportional at each instant to the remaining available energy.

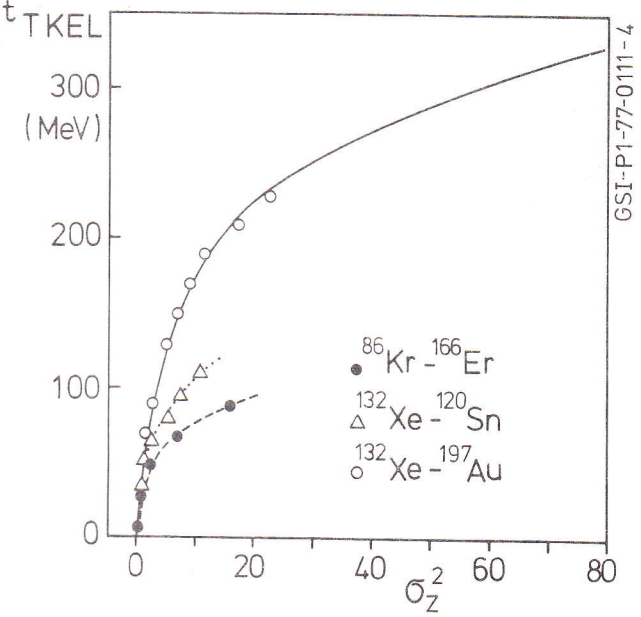

Fig.14: General relation between total kinetic energy loss and mass diffusion. The full line curve summarizes the results of Huizenga et al. (Hu 77) for the reactions Xe-Bi, Xe-Ho, Kr-Bi and Kr-Ho.

This leads to the diagram of figure 15 where σ_z^2 is plotted versus $\ln(E_0/E)$. The quantity E_0 is the total available energy and E the available energy at each moment; σ_z^2 is assumed to be a measure of the time scale. These results show that the slope depends on the total available energy, this means that the friction force (the slope gives the frictional coefficient) is not velocity dependent. At low bombarding energies the friction coefficient is larger as compared to higher energies.

An energy dependent study done for different bombarding energies, as it has been performed for Kr on Sn and Kr on Er, should be of considerable help in order to clarify the nature of the energy dissipation mechanism. The accumulated data re not yet fully analyzed, but we have learned from the presented data that the simple frictional model is not valid, that the amount of energy dissipated per exchange is too large to be accounted for by a simple frictional force. The microscopic nature of the energy dissipation remains quite an open question: is it due to particle hole excitation with the promotion of nucleons to higher shells (Wei 77), due to collective excitation including the giant mode (Wi 77), or is it just based on Q-window matching and phase space considerations?

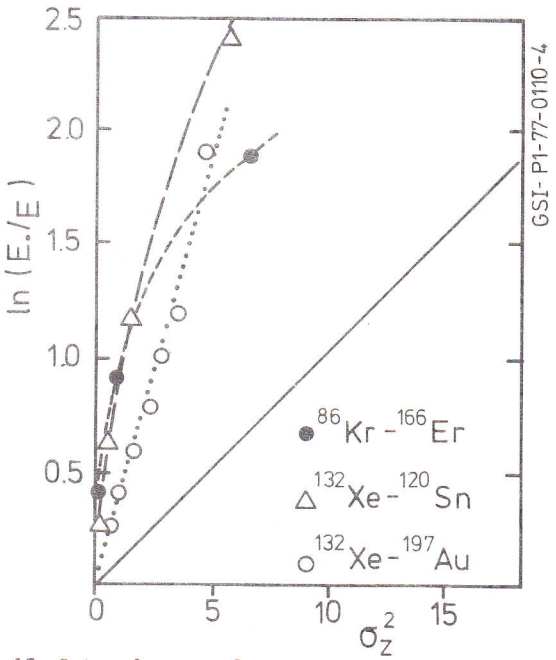

Fig.15: Rate of energy loss as a function of the number of proton exchanges. The quantity E_0 is the total available energy above the barrier, while E is the available energy for each energy loss. The straight line corresponds to the observed behaviour of the reaction Xe-Bi and Xe-Ho (Hu 76).

Additional information on the energy dissipation will be presented with the results of the γ-multiplicity measurements in the last chapter. We shall now first move on to the question of the mass diffusion for the heavier systems with the Pb-Pb, Pb-U and U-U interaction.

Until now we were considering primary products in the mass region between 80 and 200 amu, which are known from compound nucleus studies to decay predominantly by neutron emission: the measured Z-distributions were therefore fully representative of the primary Z-distributions. For nuclei with masses A >200 it is known both from compound nucleus decay studies and from the liquid drop calculations of Cohen, Plasil and Swiatecki (fig.16) that the excited fragments can easily decay by sequential fission. The aim of the present investigations is therefore on one side to delucidate if the heaviest systems follow the general trend displayed in fig. 14, to determine the primary population as a function of excitation energy in the transuranic region, and on the other side to investigate which new phenomena will occur. It is for example unknown, whether during the collision of very heavy nuclei fission will occur on a much faster time scale comparable to the interaction time, or whether the strongly deformed nuclei might favor the emission of charged particles during the collision.

The results of the three reactions U-U, U-Pb and Pb-Pb are shown in fig. 17 on a logarithmic scale for comparable observation angles and

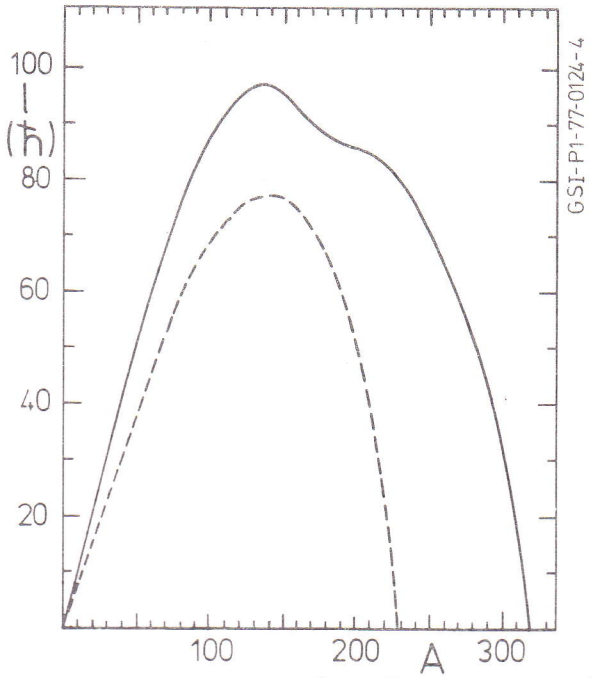

Fig.16: Liquid drop model predictions ($\omega_0/4$) of the fission barrier for Q = 0 (full line) and Q = -8 MeV. The dashed line shows where the fission-starts to compete with the neutron decay mode.

bombarding energies. In each spectrum we see after elimination of the elastically scattered events two peaks: one, close to the Z of the projectile, is narrower and asymmetric and corresponds to the normal deep inelastic scattering, whereas the second, broader, is roughly centered at half the proton number of the heavy fragments and can be associated with the sequential fission of the excited primary products (Kr 74).

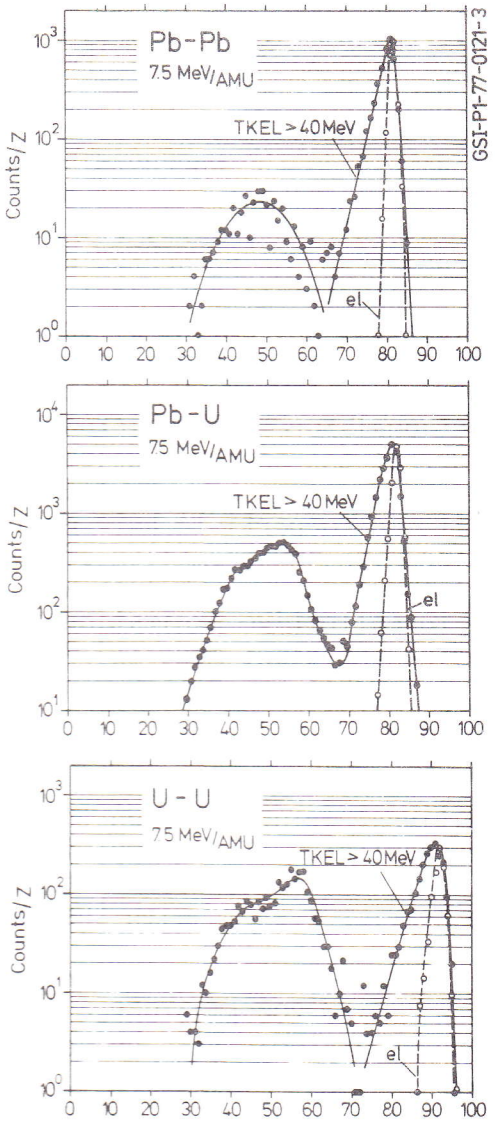

Fig.17: Overall results of the Pb-Pb, Pb-U and U-U reactions. The broad bump is originated by the sequential fission but his shape is not fully representative because the fast fission fragments are not completely stopped in the detector.

Comparing the three systems it is clear that the part of the reaction cross section which undergoes sequential fission increases with increasing mass.

The deep inelastic component has in all three cases a steep slope towards heavier elements, and a much flatter one towards lighter elements, the latter falling off much slower for U-U than for the two other reactions. The dashed lines in fig. 17 indicate the experimental resolution determined from the elastic scattering.

For comparison the Z-distribution of deep inelastic collision of Xe on Sn, where no sequential fission is observed, is shown in fig. 18.

This distribution is fully symmetric

In fig. 19 the Z-distributions for Xe-Sn and Pb-Pb are plotted for different values of TKEL. With increasing energy dissipation for Pb-Pb the distributions become more and more asymmetric, which can be explained by the fission barrier shifting to lighter nuclei. The fission probability as a function of Z can be determined from the large area recoil detector if the corresponding light reaction fragments are seen in the ionisation chamber. The results are shown in fig. 20. For the reaction Pb-Pb the fission probability rises steeply from 5 % for Z=83 to 75 % for Z=87.

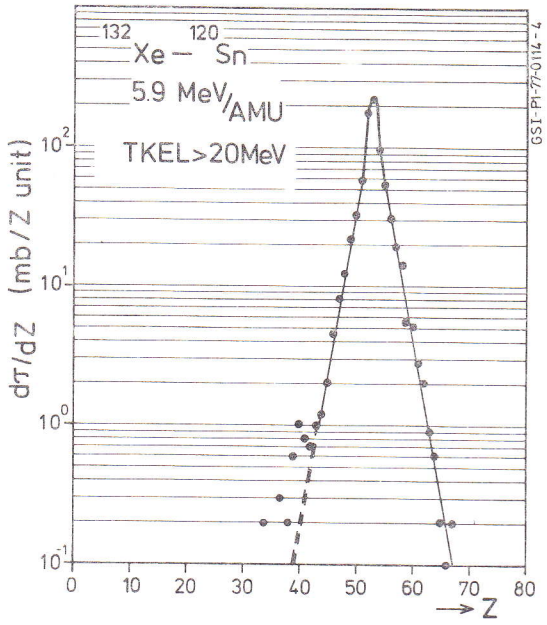

Fig.18: Same data as in figure 11a, but integrated over all non elastic events.

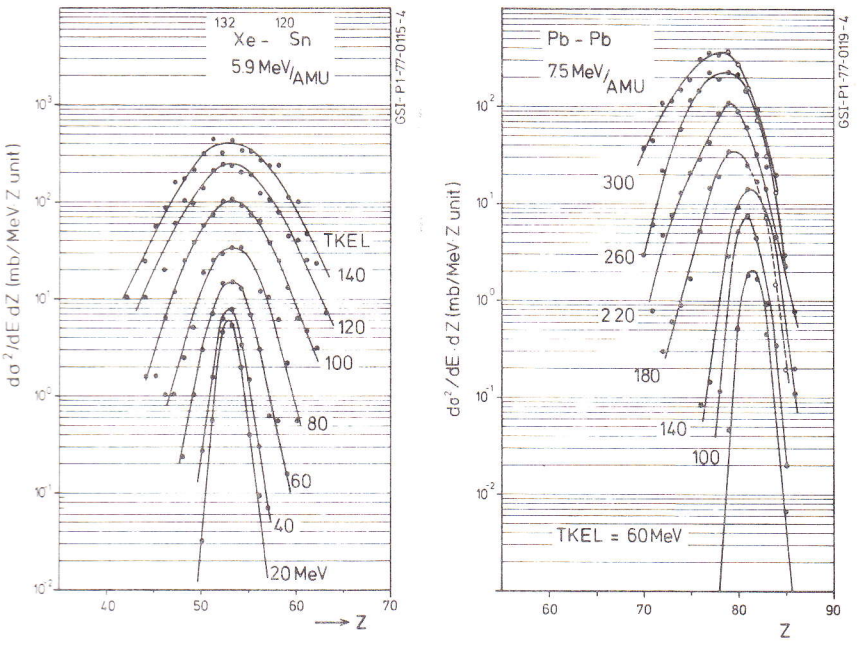

Fig.19: Proton number distributions for bins of total kinetic energy losses. The scaling factor increases from the bottom by a multiple of $\sqrt{10}$.

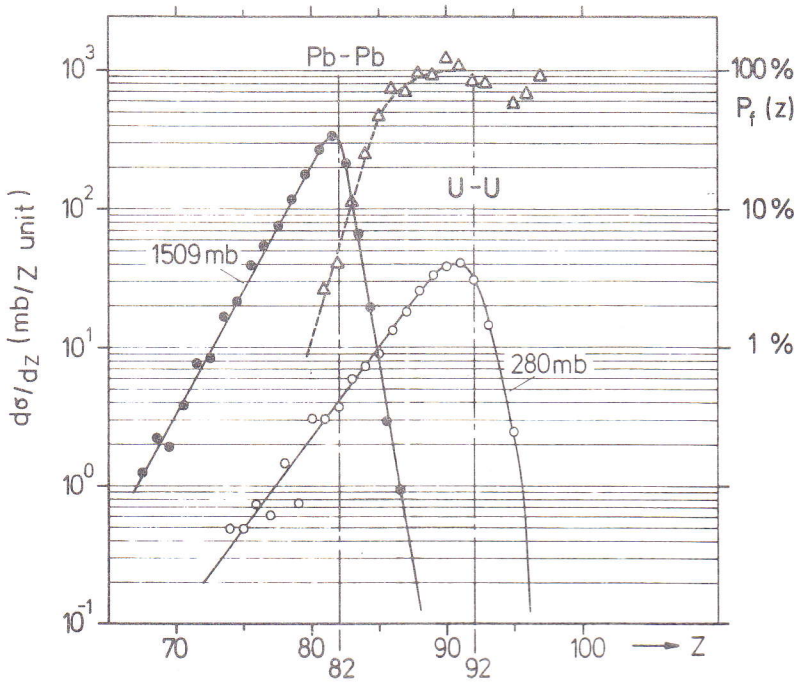

Fig.2o: The same distributions of figure 18a) and c) are compared on an enlarged Z-scale. The measured fission probability of the heavy recoil nuclei in the Pb-Pb reaction is shown by the triangles: the corresponding scale is indicated on the right side of the figure.

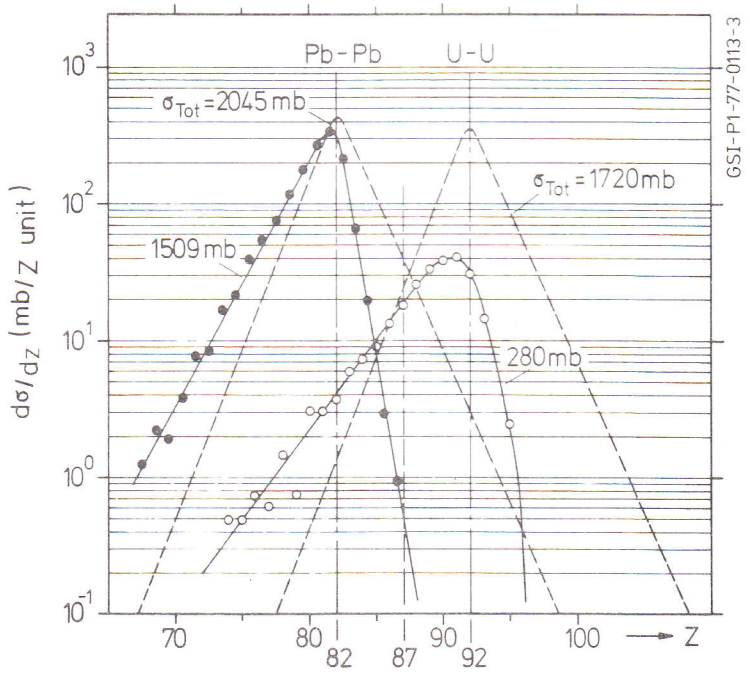

Fig.21: Primary and final distributions of the Pb-Pb and U-U reactions. The primary Z-distributions are guessed by assuming the same shape as in the Xe-Sn data of figure 19: The integral of the distribution is normalized to the total reaction cross section as determined by the grazing angle (quarter-point procedure).

In figure 21 a) the Z-distributions of the deep inelastic fragments are compared more closely for U-u and Pb-Pb. From studies performed with lighter systems, from potential energy surface arguments and especially from the fact that the two systems are symmetric, there is no reason to believe that the primary Z-distributions should not be symmetric (fig. 21). We therefore would expect similar if not identical primary yields for element Z = 87, which is in the middle between Pb and U. This intensity ratio should also not be changed by sequential fission as long as the general relation between nuclear excitation and width of the Z-distribution (fig. 14)is the same in both reactions. From fig. 21 it can however be seen that the yield of element Z = 87 is about 40 times larger in U-U than in Pb-Pb. One possible explanation would be the emission of light charged particles during or after the primary fragmentation. An alternative explanation would be that in the reaction U-U the mass transfer already occurs at lower excitation energies than in Pb-Pb. This would be of considerable importance for the production of transuranic elements and might be due to nuclear structure: Pb being doubly magic and U being deformed. Additional experiments will be performed to clarify these questions.

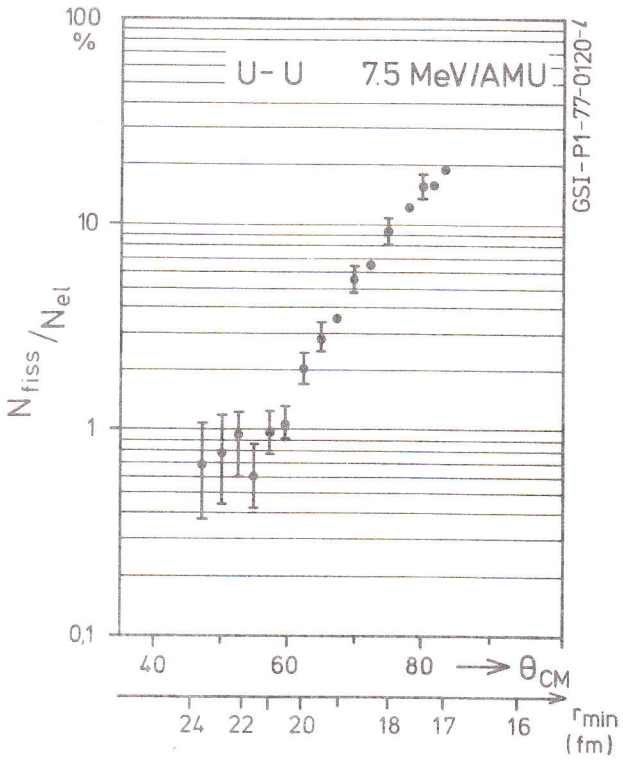

Fig.22: Coulomb fission measurement. The distance of closest approach r_{max} is evaluated for pure classical Coulomb trajectories.

The strongest possible Coulomb forces exist between two Uranium nuclei, so that this reaction is best suited for the investigation of Coulomb fission. The present measurement has been performed at a bombarding energy well above the Coulomb barrier ($E_{CM} = 1.26\ E_{Coul}$), however by selecting "elastic" scattered events at sufficiently small scattering angles (fig. 6f) it is possible to select collisions with large impact parameters for which the overlap of nuclear matter is vanishing.

The energy and angle of these "quasielastic" events have been determined with the ionisation chamber and the recoil detector (RC in fig. 1) was used to determine the fission probability of the recoiling nuclei. The measured fission probability is displayed in fig. 22.

We observe an important fission cross section even at large impact parameters. It is not possible, at present, to exclude experimentally a contribution, to the measured cross section of the subcoulomb neutron transfer induced fission. However, in our case, the contribution of such a transfer is less important on a relative scale, than the one observed in recent subcoulomb fission measurements with lighter projectiles (Co 76, Sp 77, Kr 77). Theoretical calculations (Gr 73, Wi 75, Ob 77) should be extended to this heavy system.

4. Results of the γ-multiplicity measurements

The γ-multiplicity can be considered as a measure of the total spin of the fragments after the collision, although the reconstruction of the absolute spin values from a γ-multiplicity is rather complex (Ha 75, Al 75, Ba 76, Gl 77, Pe 77, Is 76). The total spin depends on the initial angular momentum, on the slow down process and on the time scale of the interaction, which are important hidden quantities, not directly measurable: So it could turn out that the γ-multiplicty studies bring new insight into these processes and allow to distinguish between models.

We present here the results for the Kr-Sn and Kr-Er systems: they are summarized on figure 23, 24. The dependence of $\langle M_\gamma \rangle$ on angle is shown (23c) for the three branches of figure 23a: the elastic, the partly dumped and the fully relaxed. Due to tangential friction, there is a steep increase along the partly dumped component. Sticking, if any, is only achieved in the completely relaxed component. This can also be seen on figure 23d, where $\langle M_\gamma \rangle$ is plotted as a function of the TKEL. The differences in $\langle M_\gamma \rangle$ at low TKEL between Kr on Er and Kr on Sn, which have nearly equal l_{max} values indicate the presence of nuclear structure effects: the deformed Er nucleus can be easily excited in the Coulomb field, while the spherical Sn nucleus remains unexcited at large impact parameters (fig. 23c). The relation between σ_Z^2 and the TKEL of figure 14 is again displayed on figure 23b. This shows how the energy and the angular momentum are simultaneously introduced into the internal degrees of freedom of the system. The fact that for small energy loss the dissipated energy per exchange is in-

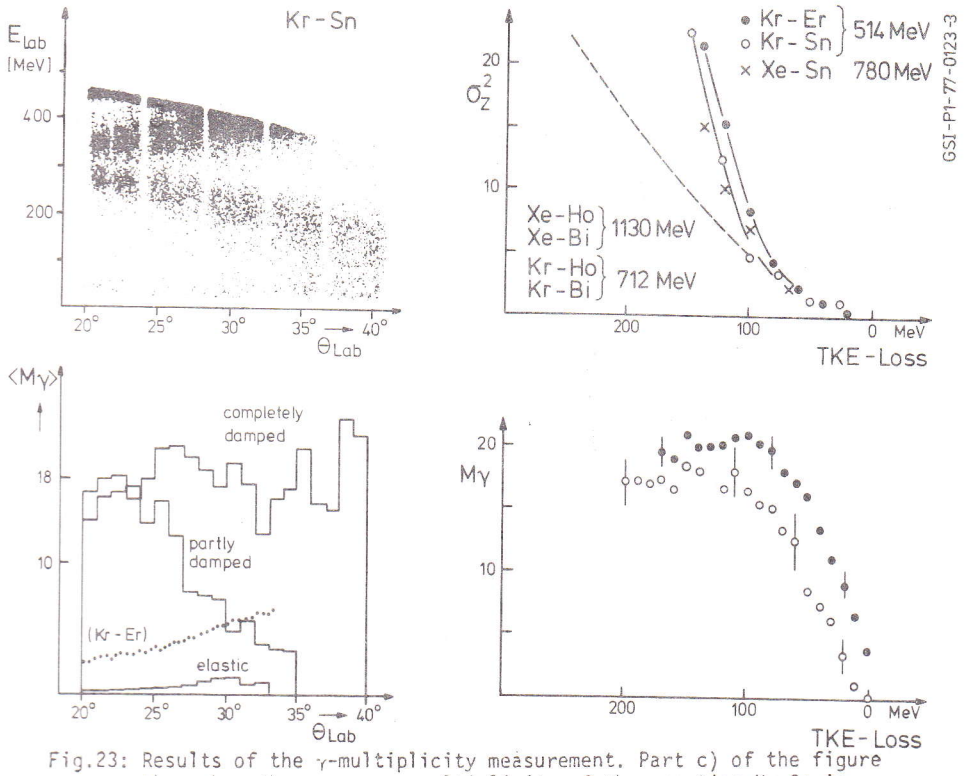

Fig.23: Results of the γ-multiplicity measurement. Part c) of the figure shows how the average γ-multiplicity of the reaction Kr-Sn increases as a function of the laboratory scattering angle for the three branches illustrated in part a): the elastic, the partly damped and the fully relaxed component. The elastic component for the reaction Kr-Er is also shown in part c) of the figure.

dependent from the bombarding energy indicates that not only velocity dependent friction forces have to be considered. This shows already a limitation of the simple classical model.

The same γ-multiplicity data of the Kr on Er reaction can also be analyzed as a function of the proton transfer. This is displayed in figure 24 for different bins of the TKEL. A dependence on the number of transferred protons is only present in the partly damped component where the system is not equilibrated. In the fully relaxed component the value of <Mγ> is independent from Z over the observed range: this is not expected in a simple sticking model picture, which predicts an increase toward asymmetric fragmentation (Bo 76).

It is of particular importance for a γ-multiplicity measurement to investigate the dependence from the impact parameter (ingoing angular momentum). Although it is difficult to associate the observed events to the ingoing angular momentum (l_{in}), a possible approach consists to integrate the observed total cross section, as a function of the TKEL, after normalization to the Rutherford scattering (Hu 77). The results of such a derivation are drawn as a full line on figure 26a. This shows that the partly damped events cover a main fraction of the total reaction cross section. If a sharp correspondence exists between l_{in} and TKEL, then the fully relaxed component has to be

associated to angular momenta smaller than 95, with an average value of 6o. The corresponding internal spin would be, in the sticking model, of about 22. This is a value much too small to explain the observed multiplicity value of 2o. It leads to two possible consequences: the nuclei are able to accomodate in the internal degree of freedom more angular momentum than the sticking model predicts or the correspondence between l_{in} and TKEL is quite broad and large impact parameters can lead to fully relaxed events. This last explanation seems to be more likely, however, the limitations of the simple classical model are disclosed here again. A number of explanations for the observed behaviour can be found in the framework of the fluctuation theory (Ngo 77) or in a microscopic quantum mechanical treatment (Wei 77, Nö 77).

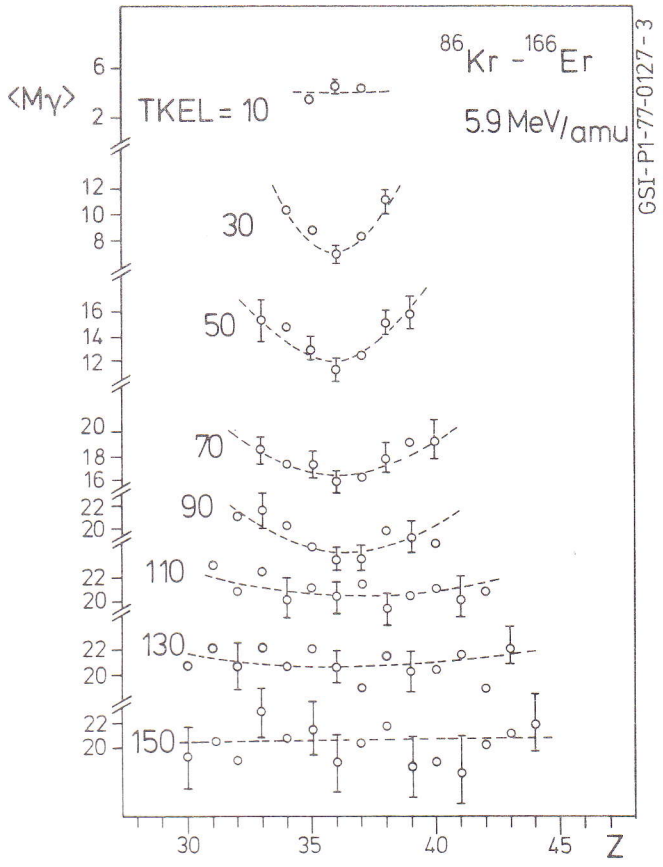

Fig.24: Dependence of the average γ-multiplicity on the total number of transferred protons.

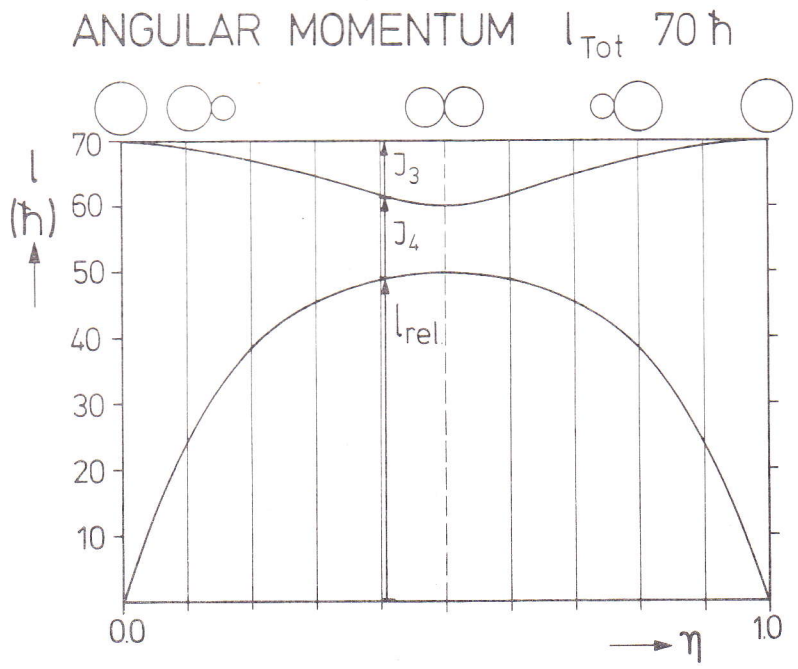

Fig.25:

Prediction of a sticking model ot two touching spheres describing the sharing of the angular momentum between internal and relative motion as a function of the asymmetry parameter $\eta=m_1/(m_1+m_2)$ for a constant total mass.

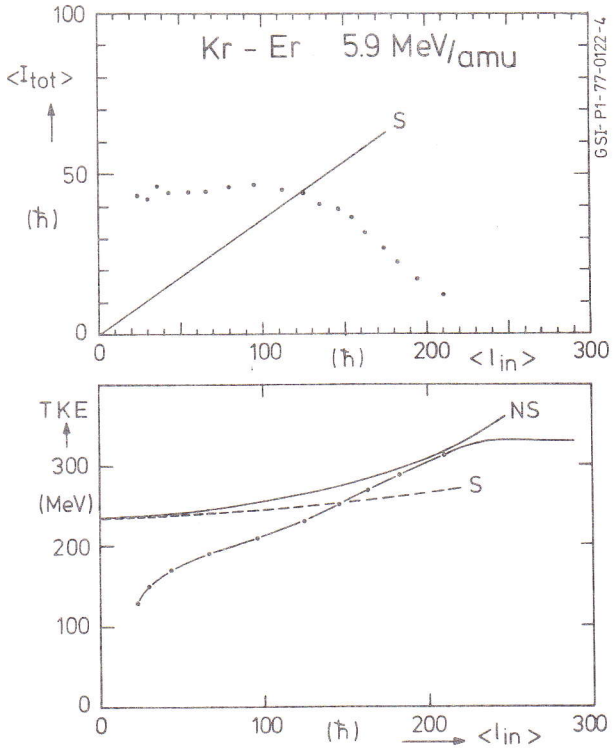

Fig.26: Comparison of the sticking model to the results of the Kr on Er reaction. Sticking is labelled by (S) non sticking by (NS). The dots of part a) were calculated from the measured γ-multiplicity by the relation $\langle l_{in} \rangle = 4 + 2 \cdot \langle M_\gamma \rangle$. The ingoing angular momentum value l_{in} was obtained from the integration of the cross section in bins of the TKEL.

Another interesting information, which can be derived from the data consists in associating the observed low kinetic energies to the deformation at the scission point. In figure 25a are indicated the barrier heights for two touching spheres ($R = 1.50 \{A_1^{1/3} + A_2^{1/3}\}$) in a non sticking (NS) and in a sticking configuration (S). The observed TKE is small, which suggests that deformation effects can be of importance, not only in the fully relaxed component but even at an earlier stage in the partially damped component. This can be interpreted in terms of cojlective excitation modes (Wi 77) or in terms of a neck formation between elongated fragments (Bo 77).

Conclusions

A systematic survey of deep inelastic reactions was performed for colliding nuclei of masses between 8o and 24o amu.

The application of large surface detectors and, particularly, of a position sensitive ionisation chamber, has proved to be very effective and appropriate for this type of investigations.

The Wilczynski diagrams describing the relative motion between the colliding objects shows a gradual trend as a function of growing masses of target and projectile where the trajectories lead the particles not toward negative scattering angles but increasingly into the direction around and above the grazing angle. We attribute this behaviour to a delicate balance between Coulomb and nuclear forces.

The energy dumping as a function of the mass transfer strength matches a general law between total kinetic energy loss and the variance of the proton number distribution. For the partly damped component this relation seems to hold independently from the choice of ingoing channel and bombarding energy. The dissipation of the kinetic energy does not depend only on the relative velocity of the impinging nuclei, and the simple friction model is not appropriate to describe these processes.

The γ-multiplicity measurement displays a rapid increase as a function of scattering angle and total kinetic energy loss, which give new insights to the process and indicate the necessity of microscopic quantum mechanical calculations of the interaction.

In the U-U collision large mass transfers are present which possibly populate with relatively large cross sections the transuranic elements. In the Pb-Pb reaction the mass transfer is more restricted. The decay probability by fission of the primary masses increases strongly for growing masses and excitation energies. The presented investigations are by no means completed and hold promise of additional surprises and excitements.

Acknowledgements

The authors would like to thank the staff of the UNILAC accelerator for providing unique ion beams and D. Maier, M. Ludwig,and H.J. Beeskov for their technical support and H. Folger for the preparation of a variety of excellent targets. The assistance of P. Rother and collaborators for the off-line data reduction is gratefully acknowledged. It is a pleasure to thank Dr. Sven Björnholm for many fruitful discussions.

References

Al 75 R. Albrecht, W. Dünnweber, G. Graw, H. Ho, S.G. Steadman, and J.P. Wurm, Phys. Rev. Lett. 34, 1400 (1975)

Ar 73 A.G. Artukh, G.F. Gridnev, V.L.Mikheev, V.V. Volkov, and J. Wilczynski, Nucl. Phys. A215, 91 (1973)

Be 69 K. Beyer and A. Winther, Phys. Lett. B 30, 296 (1969)

Bo 77 R. Bock, B. Fischer, A. Gobbi, K. Hildenbrand, W. Kohl, U. Lynen, I. Rode, H. Stelzer, G. Auger, J. Galin, J.M. Lagrange, R. Albrecht, B.B. Back, IX Masurian School in Nuclear Physics, published in Nucteonica (1977)

Br 76 R.A. Broglia, C.H. Dasso and Aa. Winther, Phys. Lett. 61B, 113 (1976)

Co 74 S. Cohen, F. Plasil, W.J. Swiatecki, Annals of Physics, 82, 557 (1974)

Co 76 P. Colombani, P.A. Butler, I.Y. Lee, D. Cline, R.M. Diamond, F.S. Stephens and D. Ward, Phys. Lett. B 65, 39 (1976)

De 75 H.H. Deubler, K. Dietrich, Phys. Lett 56B, 241 (1975)

Fr 77 G. Franz, H. Ahrens, W. Brüchle, H. Folger, J.-V. Kratz, M. Schädel, I. Warnecke, G. Wirth, GSI Annual Report 1976

Ga 76 G. Galin, European Conference on Physics with Heavy Ions. CAEN J. Physique (1976)

GSI 76 GSI, Annual Report 1976

Ha 75 G.B. Hagemann, R. Broda, B. Herskind, M. Ishihava, S. OGaza, H. Ryde, Nucl. Phys. A245, 166 (1975)

Ha 77 D. Habs, V. Metag, J. Schukraft, H.J. Specht, C.O. Wene, K.D. Hildenbrand, submitted for publication in Zeitschrift für Physik (1977)

Ho 72 H. Holm and W. Greiner, Nucl. Phys. A 195, 333 (1972)

Hu 76 J.R. Huizenga, J.R. Birkelund, W.U. Schroeder, K.L. Wolf, V.E. Viola, Phys. Rev. Lett. 37, 885 (1976) and J.R. Huizenga Erda Report Coo3496-56

Hu 77 J.R. Huizenga, W.U. Schröder, Ann. Rev. Nucl. Sci. 27 (1977)

Is 76 M. Ishihara, T. Numao, T. Fukuda, K. Tanaka, and I. Inamura, in Proceedings of the Symposium on Macroscopic Features of Heavy-Ion Collisions, Argonne, Illinois, 1976, edited by D.G. Kovar, ANL Report No. ANL/PHY 76-2, p. 617

Kr 74 J.V. Kratz, A.E. Norris, and G.T. Seaborg, Phys. Rev. Lett. 33, 5o2 (1974)

Kr 77 J.V. Kratz et al., GSI, Annual Report 1976

Le 76 M. Lefort, Symposium on New Avenues in Nuclear Physics, Rehovot (Israel) Nov. 7-9, 1976

Mo 76 L.G. Moretto, LBL 5o57 European Conference on Physics with Heavy Ions CAEN (1976)

L.G. Moretto, B. Cauvin, P. Classel, R. Jared, P. Russo, J. Sventck, G. Wozniak, Phys. Rev. Lett. 36, 1o69 (1976)

Ng 77 C. Ngô, H. Hofmann, this Conference

Nö 76 W. Nörenberg, European Conference on Physics with Heavy Ions, Caen, 1976

Ob 77 V. Oberacker, G. Soff and W. Greiner, preprint

Pe 77 N. Perrin, J. Peter, Institut de Physique Nucléaire, Orsay, preprint

Re 77 R. Renfordt, GSI Annual Report, 1976.

Sa 75 H. Sann, Nucl. Instr. al.Meth 124, 5o9 (1975)

St 76 H. Stelzer, GSI Annual Report, 1976.
H. Stelzer, Nucl. Instr. al.Meth. 138, 4o9 (1976)

Wei 77 H. Weidenmüller, this Conference

Wi 77 J. Wilczynski, Phys. Lett. 47A, 484 (1973).